THE JOURNAL OF PHYSICAL CHEMISTRY A

Article

pubs.acs.org/JPCA

Velocity Map Imaging Study of Ion−Radical Chemistry: Charge Transfer and Carbon−Carbon Bond Formation in the Reactions of Allyl Radicals with C^+

Linsen Pei and James M. Farrar*

Department of Chemistry, University of Rochester, Rochester, New York 14627, United States

Supporting Information

ABSTRACT: We present an experimental and computational study of the dynamics of collisions of ground state carbon cations with allyl radicals, C_3H_5, at a collision energy of 2.2 eV. Charge transfer to produce the allyl cation, $C_3H_5^+$, is exoergic by 3.08 eV and proceeds via energy resonance such that the electron transfer occurs without a significant change in nuclear velocities. The products have sufficient energy to undergo the dissociation process $C_3H_5^+ \rightarrow C_3H_4^+ + H$. Approximately 80% of the reaction products are ascribed to charge transfer, with ∼40% of those products decaying via loss of a hydrogen atom. We also observe products arising from the formation of new carbon−carbon bonds. The experimental velocity space flux distributions for the four-carbon products are symmetric about the centroid of the reactants, providing direct evidence that the products are mediated by formation of a $C_4H_5^+$ complex living at least a few rotational periods. The primary four-carbon reaction products are formed by elimination of molecular hydrogen from the $C_4H_5^+$ complex. More than 75% of the nascent $C_4H_3^+$ products decay by C−H bond cleavage to yield a $C_4H_2^+$ species. Quantum chemical calculations at the MP2/6-311+g(d,p) level of theory support the formation of a nonplanar cyclic $C_4H_5^+$ adduct that is produced when the p-orbital containing the unpaired electron on C^+ overlaps with the unpaired spin density on the terminal carbon atoms in allyl. Product formation then occurs by 1,2-elimination of molecular hydrogen from the cyclic intermediate to form a planar cyclic $C_4H_3^+$ product. The large rearrangement in geometry as the $C_4H_3^+$ products are formed is consistent with high vibrational excitation in that product and supports the observation that the majority of those products decay to form the $C_4H_2^+$ species.

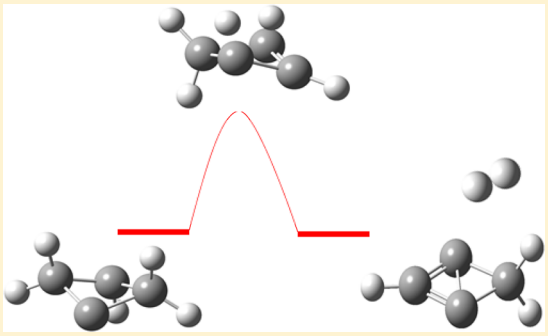

INTRODUCTION

The study of reactions of ions with stable atoms and molecules occupies an important position in the field of chemical dynamics, devoted to answering the question "Where does the energy go in a chemical reaction?" The quest to understand how chemical reactions occur at the level of the underlying potential energy surface is characterized by the conflicting requirements of more precise specification of the initial conditions of an experiment, i.e., reactant quantum state preparation and product detection, and a desire to expand the chemical diversity of species probed at this level of sophistication. The velocity map imaging (VMI) method[1] has begun to play an important role in this evolution because the signal levels afforded by the detection of all velocity space elements in a single time window, i.e., multiplex advantage, are compatible with products formed in low concentrations.

The development of a reliable, intense source of free radicals,[2,3] based on supersonic expansion of gas containing an appropriate radical precursor and subsequent pyrolysis in a heated SiC "afterburner", has made the study of reactions of free radicals in crossed molecular beams possible. Pioneering crossed beam studies of the reactions of free radicals with open-shell atoms[4−9] have revealed new patterns of reactivity and dynamical signatures, and the rich chemistry observed has been supported by significant theoretical efforts.[9−11]

Only recently has the subject of the reactions of ions with free radicals received experimental attention. Russell et al.[12] reported a Fourier transform ion cyclotron resonance study of the reactions of the benzyl cation with allyl radicals that provided evidence for the formation of new C−C bonds. Ellison and Bierbaum and their co-workers[13,14] have measured rates of proton transfer from H_3O^+ to allyl radicals and benzyne diradicals in a SIFT (selected ion flow tube) experiment. Most recently, the Viggiano lab[15] showed that reactions of Ar^+ and O_2^+ with CH_3 radicals were dominated by charge transfer, consistent with the low ionization energies of free radicals. A recent publication from our laboratory[16] in which an ion beam was crossed by a beam of free radicals produced by pyrolysis and products were detected by VMI, examined both the proton transfer and charge transfer reaction of H_3^+ with CH_3. The study reported one of the first probes of energy partitioning in ion−radical reactions, examining not only the ubiquitous

Received: June 6, 2016
Revised: July 19, 2016
Published: July 19, 2016

DOI: 10.1021/acs.jpca.6b05699
J. Phys. Chem. A 2016, 120, 6122−6128

process of charge transfer but also proton transfer, a process that is often governed by both kinematics and dynamics.[17]

In an initial attempt to probe the rich chemistry of bond formation reactions that may occur between ions and hydrocarbon-based free radicals, we have examined collisions of the ground state carbon cation with allyl radical in this paper. The specific reactions observed in this study are the following:

$$C^+(^2P) + C_3H_5 \rightarrow C_3H_5^+ + C \quad \Delta H^\circ = -3.08\ \text{eV} \quad (1)$$

$$\rightarrow C_3H_4^+ + H + C \quad \Delta H^\circ = +0.62\ \text{eV} \quad (2)$$

$$\rightarrow c\text{-}C_4H_3^+ + H_2 \quad \Delta H^\circ = -7.20\ \text{eV} \quad (3a)$$

$$\rightarrow n\text{-}C_4H_3^+ + H_2 \quad \Delta H^\circ = -7.49\ \text{eV} \quad (3b)$$

$$\rightarrow c\text{-}C_4H_2^+ + H + H_2 \quad \Delta H^\circ = -1.91\ \text{eV} \quad (4a)$$

$$\rightarrow n\text{-}C_4H_2^+ + H + H_2 \quad \Delta H^\circ = -3.55\ \text{eV} \quad (4b)$$

Both charge transfer and carbon−carbon bond formation processes occur, each of which forms products with sufficient internal energy to cleave a C−H bond in the most highly internally excited parent ions. The reaction exoergicity for (1) is calculated from standard enthalpies of formation taken from the literature.[18] The reaction exoergicities for (2), (3a,b), and (4a,b) are estimated from *ab initio* calculations described in a later section of this paper. The prefixes c and n denote cyclic and open-chain products, respectively.

EXPERIMENTAL METHOD

The crossed beam experimental arrangement has been described in our previous publications.[19,20] The charged and neutral reactant beams intersect in a grounded region of space electrostatically shielded by electrodes with a cylindrical "curtain" design similar to that described by Wester and co-workers.[21] Reaction products are ejected from the collision volume by a short electrical pulse that initiates the VMI detection process. A series of aperture lenses held at appropriate potentials provides the electrostatic fields that satisfy the velocity mapping condition and correct for the chromatic aberration that arises from the finite thickness of the collision volume. The products travel along a 0.6 m drift space, strike a pair of microchannel plates (MCPs) mounted in a chevron configuration, and produce an image that is displayed on a phosphor screen. The MCPs are gated with an appropriately delayed pulse that is correlated with the flight time of product ions. A charge-coupled device (CCD) camera records this image and sends the digital output to a laboratory computer via a USB interface. The shielded volume in which the beams intersect is maintained at a pressure 2×10^{-7} Torr with both beams running. The ion detector is differentially pumped with a turbomolecular pump.

The free radical source is based on the afterburner design described above. A pulsed solenoid valve injects a 1% mixture of 1,5-hexadiene (Aldrich) in He carrier gas at a total pressure of 3 atm into a 1 mm diameter SiC tube 25 mm in length heated by 45 W of dc power. The flow from the pyrolysis region is sonic under these operating conditions.[22] Experiments were carried out to ensure that all product ions were formed from C_3H_5 radicals produced pyrolytically rather than from undissociated precursor species. The internal temperature of the allyl radicals is estimated to be approximately 500 ± 100 K, on the basis of results from a recent synchrotron radiation study of the threshold photoelectron spectroscopy of radicals produced from a continuous pyrolytic source with similar heating parameters.[23] The internal energy contribution to the system from the radical beam is thus considered to be small, on the order of 0.05 eV, consistent with the results of crossed beam studies of allyl radicals with oxygen atoms.[5]

The ion beam is produced by electron impact on a 10% mixture of CO in He in the ion source described in the literature,[24] and employed in previous studies from our lab.[19,20] This method is known to produce carbon cations in the ground (^2P) electronic state with excited state contamination below 1%.[25,26] The ion beam is extracted from the source and is momentum-analyzed, focused, and decelerated to its terminal energy at the collision center, which is maintained at ground potential as described previously. The energy width of the ion beam is ∼0.2 eV full width half-maximum (fwhm).

RESULTS

Velocity map images for all products are determined as described in previous publications.[19,20] Figure 1 shows raw velocity map images for charge transfer (m/e = 41) and dissociative charge transfer (m/e = 40) products, reactions 1 and 2, at a collision energy of 2.2 eV. Figure 2 shows the ion

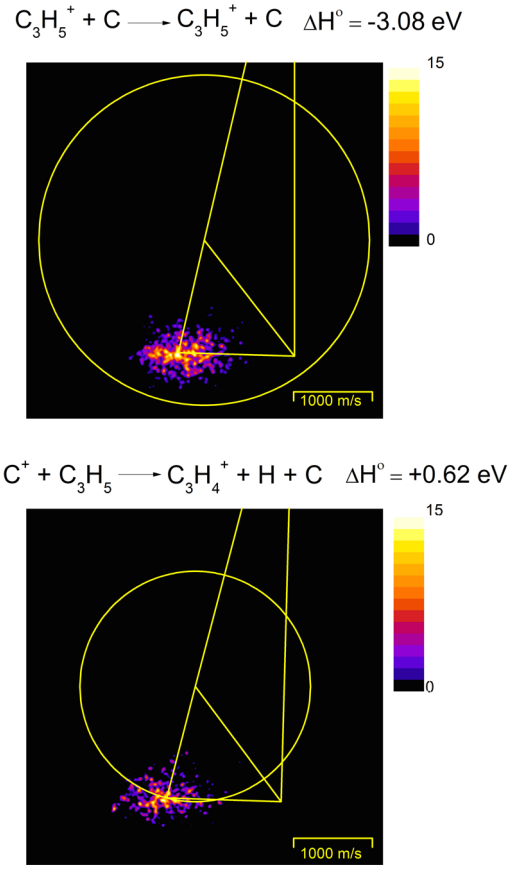

Figure 1. Top panel: velocity map image for $C_3H_5^+$ charge transfer products at collision energy of 2.2 eV. The kinematic Newton diagram appropriate for this collision energy is superimposed on the image. The circle describes the maximum charge transfer product center of mass speed allowed by the sum of collision energy and reaction endoergicity. Bottom panel: same as above, for $C_3H_4^+$ dissociative charge transfer products at collision energy of 2.2 eV.

DOI: 10.1021/acs.jpca.6b05699
J. Phys. Chem. A 2016, 120, 6122−6128

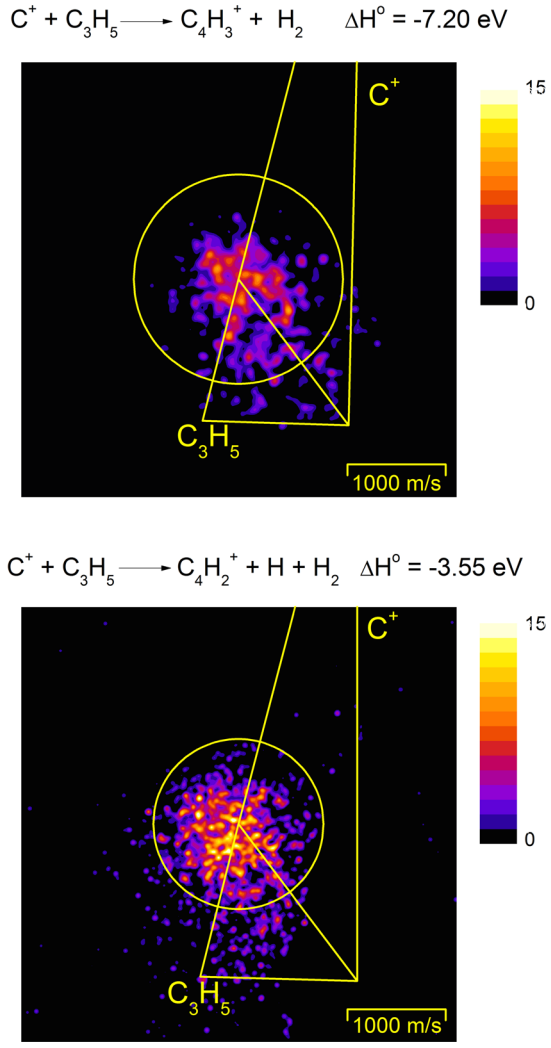

Figure 2. Top panel: velocity map image for $C_4H_3^+$ bond formation products at a collision energy of 2.2 eV. The kinematic Newton diagram appropriate for this collision energy is superimposed on the image. The circle describes the maximum $C_4H_3^+$ product center of mass speed allowed by the total available energy, the sum of collision energy and reaction endoergicity. Bottom panel: same as above, for $C_4H_2^+$ bond formation products at a collision energy of 2.2 eV.

images for the formation of the carbon−carbon bond formation reactions to produce $C_4H_3^+$ (m/e = 51) and $C_4H_2^+$ (m/e = 50), reactions 3a,b and 4a,b. The images represent Cartesian flux in center of mass coordinates, denoted $P(u_x,u_y)$.[27] Kinematic Newton diagrams appropriate for each of the collision energies are superimposed on the images.

The images for charge transfer, which show maximum intensity at the tip of the neutral free radical velocity vector, provide clear evidence that electron transfer is a direct process occurring at long range and that the momenta of the product ion and neutral reactant are sensibly equal. The images for the formation of $C_4H_3^+$ and $C_4H_2^+$, in contrast, are localized around the centroid of the collision system and suggest that the formation of those products occurs through a reactive intermediate that lives at least several rotational periods.

An important observation associated with the relative signal levels of reactions 1−4 is that the primary reaction products arise from charge transfer. Roughly 80% of the total product yield corresponds to charge transfer, reactions 1 and 2. This result is consistent with the preeminence of charge transfer as a major channel in much of gas phase ion chemistry. Approximately 40% of the nascent charge transfer products dissociate to form $C_3H_4^+$, consistent with the fact that nearly 6 eV is accessible to the $C_3H_5^+$ product. Perhaps more surprising is the fact that of the remaining reaction products formed by carbon−carbon bond formation, only ∼20% of those products survive as $C_4H_3^+$.

The Cartesian flux profiles shown in Figures 1 and 2 were processed by inverse Abel transformation to extract proper product velocity and kinetic energy distributions. We have employed the BASEX program[28] for this purpose. The transformed data may then be expressed in barycentric polar coordinates u and θ, given by the following expressions:

$$u = (u_x^{\,2} + u_y^{\,2})^{1/2} \tag{5}$$

$$\theta = \tan^{-1}(u_y/u_x) \tag{6}$$

The relationship between Cartesian and polar flux intensity is then simply found from the following relationship:

$$I_{cm}(u,\theta) = u^2 P(u_x,u_y) \tag{7}$$

Product angular and kinetic energy distributions are computed by integrating the flux distributions over recoil speed and scattering angle, respectively. The angle-averaged relative translational energy distribution of products, $P(E_T')$, is given by the following expression:

$$\langle P(E_T')\rangle_\theta = \int_0^\pi d\theta \sin\theta\, u P(u_x,u_y) \tag{8}$$

Integration over specific angular regions provides a means to assess how energy disposal may depend on scattering angle. Even in the case of a collision complex that lives at least several rotational periods, one might expect the angular distribution to be coupled to the recoil energy distribution, especially when hydrogen atoms are ejected, but the quality of the data reported here are insufficient to justify such an analysis.

The total energy accessible to the reaction products is defined as

$$E_{total} = E_T + E_{int} - \Delta H \tag{9}$$

where E_T is the initial relative kinetic energy, E_{int} is the total internal energy of the reactants, and ΔH is reaction exoergicity. As we noted earlier, the neutral reactants are formed with relatively low internal energy below 0.1 eV.[5]

The product kinetic energy distributions for the charge transfer processes (1) and (2) are shown in Figure 3, and Figure 4 shows the corresponding distributions for the carbon−carbon bond formation processes (3a,b) and (4a,b). Apparent structure in the distributions is within the error limits shown on the figures, reflective of the low signal levels in these experiments. The red curves shown in the plots are simply to guide the eye. The kinetic energy distributions for charge transfer are consistent with electron transfer occurring on a time scale sufficiently short that the velocities of the C_3H_5 reactants and $C_3H_5^+$ products are the same. The distributions for carbon−carbon bond formation are strongly peaked at low kinetic energy, consistent with disposal of a small fraction of the available energy into product translation. The kinetic energy distributions for the primary $C_4H_3^+$ products resemble those for the dissociation products $C_4H_2^+$ + H, although less total energy is accessible to the latter products. This fact is reflected in the

DOI: 10.1021/acs.jpca.6b05699
J. Phys. Chem. A 2016, 120, 6122−6128

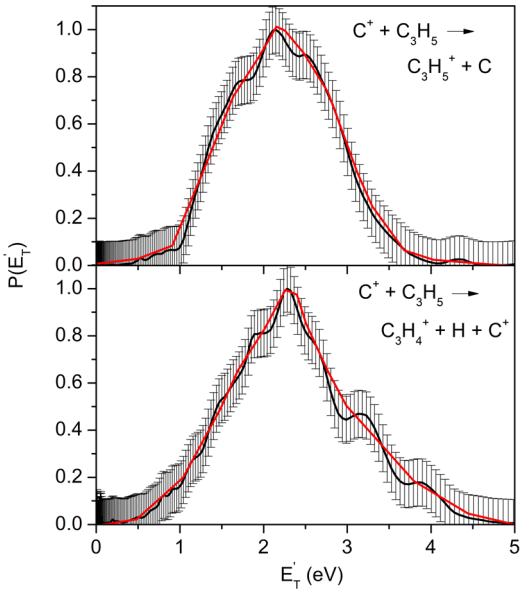

Figure 3. (a) Product kinetic energy distribution for the $C_3H_5^+$ products at a collision energy of 2.2 eV. Error bars signify error limits based on counting statistics for products formed at a given collision energy. The red curve is provided to "guide the eye" in interpreting the distributions and its error limits. (b) Same as in (a), for $C_3H_4^+$ formation.

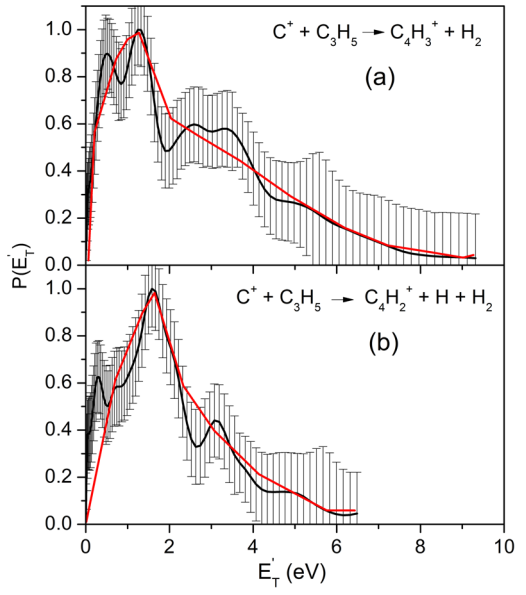

Figure 4. (a) Product kinetic energy distribution for the $C_4H_3^+$ products at a collision energy of 2.2 eV. Error bars signify error limits based on counting statistics for products formed at a given collision energy. The red curve is provided to "guide the eye" in interpreting the distributions and its error limits. (b) Same as in (a), for the $C_4H_2^+$ products at a collision energy of 2.2 eV.

images shown in Figure 2, where the velocity space circle defining the maximum speed for the $C_4H_2^+$ products is smaller than for $C_4H_3^+$ products. However, the images for both products fall cleanly within the circles defining the respective thermodynamic limits, whether the products are cyclic or open chain. Kinetic energy release data alone are insufficient to distinguish between these two isomeric forms.

Formation of $C_4H_2^+ + H_2 + H$ is a three-body process. We have estimated the kinetic energy for formation of the $C_4H_2^+$ product shown in Figure 4b by assuming that this product is formed by ejection of a hydrogen atom from the $C_4H_3^+$ product with small kinetic energy. Thus, the velocity of the nascent $C_4H_2^+$ product is essentially equal to that of the parent $C_4H_3^+$ precursor. This procedure is well-established and has been validated in the literature.[29−31]

COMPUTATIONAL STUDIES

The experimental velocity map image for the formation of the $C_4H_3^+$ product is symmetric with respect to the centroid of the collision system, providing evidence that the approaching reactants form a long-lived $C_4H_5^+$ reactive intermediate from which product formation occurs by ejection of two hydrogen atoms. Computations described in this section will show that that spin-allowed elimination of molecular hydrogen is likely the preferred route for $C_4H_3^+$ production. The nature of the interaction of the $C^+(^2P)$ reactant with the π-type molecular orbitals of the allyl radical provides qualitative justification for the role of a $C_4H_5^+$ intermediate living at least a few rotational periods and formed by the approaching reactants. The singly occupied molecular orbital (SOMO) of allyl is nonbonding, with a node on the central carbon atom and out-of-phase p-orbitals on the terminal carbon atoms. The incoming C^+ reactant may approach the allyl radical perpendicular to the plane of the carbon atoms, and overlap of the wave function for the single 2p-electron on C^+ with the SOMO produces a nonplanar cyclobutyl ring system.

This simple picture may be justified with rigorous calculations. A computational study of nine isomers of $C_4H_5^+$ reported by Cunje et al.[32] has identified a number of isomerization pathways among linear and cyclic structures and offers us a starting point for understanding possible routes to $C_4H_3^+$ products from a $C_4H_5^+$ structure assembled from the reactants. Our calculations, performed via the MP2 method with the 6-11+g(d,p) basis set in Gaussian 03,[33] produced structures of reactants, products, reactive intermediates, and transition states connecting selected $C_4H_5^+$ intermediates. An intrinsic reaction coordinate (IRC) calculation for each transition state (TS) verified that the TS in question connected the appropriate intermediates. Details of the structures obtained by the computations are reported in the Supporting Information for this article.

A potential energy surface scan showed, as expected, that the preferred carbon cation approach is perpendicular to the plane defined by the three carbon atoms of the allyl radical, with the C^+ p-orbital oriented in a plane parallel to the allylic framework. This approach geometry allows the electron density on the carbon cation to overlap the unpaired spin densities on the terminal carbon atoms of allyl, forming a four-membered ring. This species corresponds to structure **13** of Cunje et al.[32] The carbon atom framework of this intermediate is non-coplanar, forming a butterfly-shaped structure. The calculations also showed that the carbon cation does not attack the unpaired spin density presented by a terminal carbon on allyl to produce an open-chain intermediate.

Figure 5 summarizes the results of these *ab initio* calculations, as detailed in the Supporting Information. Figure 5a shows the formation pathway for the cyclic isomer of $C_4H_3^+$. Figure 5b illustrates the pathway for forming open-chain $C_4H_3^+$ products. The terminal carbon atoms of the allyl radical are labeled C_1 and C_3, the central carbon is denoted C_2, and the approaching

DOI: 10.1021/acs.jpca.6b05699
J. Phys. Chem. A 2016, 120, 6122−6128

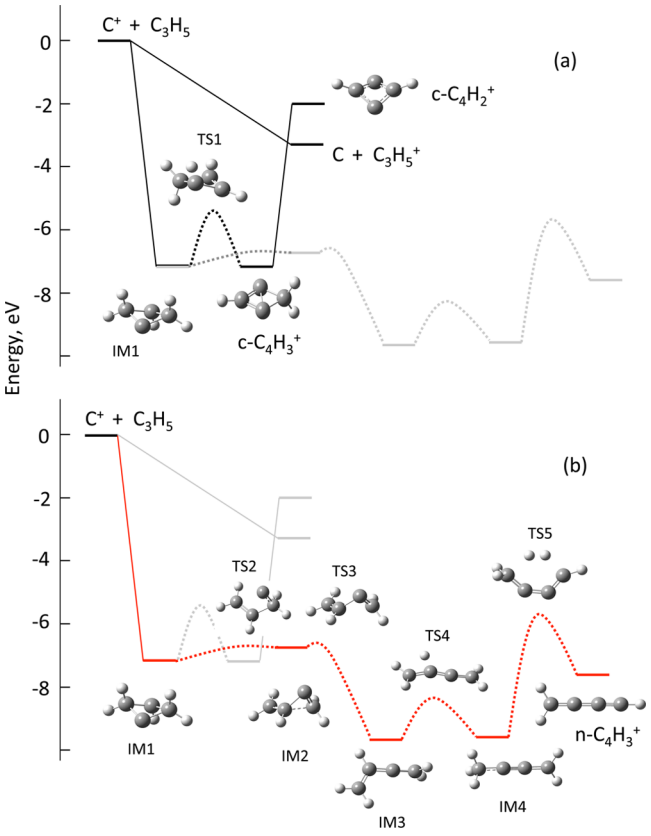

Figure 5. (a) Reaction coordinate diagram summarizing the *ab initio* pathway for the production of cyclic $C_4H_3^+$ and $C_4H_2^+$ products. Details of the structures of **IM1**, **TS1**, and the products are given in the Supporting Information. (b) Reaction coordinate diagram summarizing the *ab initio* pathway for the production of open-chain $C_4H_3^+$ products. Details of the structures of intermediates (**IM**–**IM4**), transition states (**TS2**–**TS5**), and the products are given in the Supporting Information.

carbon cation corresponds to C_4. These assignments are indicated clearly in the structures reported in the Supporting Information.

As noted earlier, approach of C^+ perpendicular to the plane defined by the allyl carbon atoms results in the formation of **IM1**. The newly formed C_1–C_4 and C_3–C_4 bond lengths are both 1.53 Å, and the C_1–C_4–C_3 bond angle is 96.75°. The dihedral angle between the $(C_1C_2C_3)$ and $(C_1C_4C_3)$ planes, which defines the degree of non-coplanarity in **IM1**, is 138°. Formation of the four-membered ring causes the C_1–C_2–C_3 angle to decrease from its value of 124° in allyl to 104° in **IM1**. The carbon–carbon bond lengths increase from 1.38 Å in allyl to 1.46 Å in **IM1**. The calculation shows that the intermediate **IM1** lies 7.11 eV below the reactants.

The intermediate **IM1** may undergo 1,2-elimination of molecular hydrogen through transition state **TS1** over a 1.75 eV barrier to form a cyclic $C_4H_3^+$ product, which lies 7.2 eV below the reactants. The elimination of molecular hydrogen across the C_1–C_2 bond results in a shortening of the bond from 1.46 to 1.37 Å, consistent with the conversion of the single bond to a double bond. The carbon skeleton of the cyclic $C_4H_3^+$ product is planar, indicative of major geometric reorganization, and suggesting that the product is highly vibrationally excited. This observation has major implications for energy disposal in the carbon–carbon bond formation reaction and subsequent dissociation of the nascent product.

A recent study of the photoelectron spectra of neutral C_4H_5 radicals[34] demonstrated that $C_4H_5^+$ ions may exist as open-chain isomers in addition to the cyclic species identified by Cunje et al.[32] This observation motivated us to search for reactive pathways between C^+ and allyl radicals that form open-chain products and result in elimination of hydrogen atoms or molecules.

The calculations revealed that the cyclic intermediate **IM1** may also undergo a series of rearrangements that ultimately leads to a linear isomer of $C_4H_3^+$. Figure 5b illustrates the processes involved. Attack of C_4 on C_2, with an activation barrier of 0.44 eV, followed by cleavage of the C_4–C_1 bond produces an intermediate **IM2** that is best described as a distorted methylene cyclopropane ring system. The C_2–C_3 bond, which is abnormally long in **IM2**, 1.71 Å, ultimately cleaves over a small barrier (~0.08 eV) to form an open-chain intermediate, denoted **IM3**, that lies nearly 3 eV below **IM1** and **IM2** and is the lowest energy structure in the pathway for producing open-chain products. Hydrogen atom migration in **IM3** from C_2 to C_1 over a 1.53 eV barrier forms **IM4**, which corresponds to structure **4** in the work of Cunje et al.[32] The calculations indicate that 1,4-elimination of H_2 over a 3.68 eV barrier leads to the linear H_2CCCCH isomer of $C_4H_3^+$. This product is ~0.9 eV more stable than the cyclic $C_4H_3^+$ product, but the long sequence of rearrangements that precedes its formation, with the tight transition state associated with the high barrier for H_2 elimination, suggests that this pathway is significantly less probable than simple elimination of H_2 from **IM1**.

In support of this hypothesis, rate constants for isomerization of selected intermediates that control the branching between cyclic and open-chain $C_4H_3^+$ products were computed with the statistical Rice–Ramsperger–Kassel–Marcus prescription[35] using the vibrational frequencies for the relevant intermediates and transition states connecting them. At the total energy available to nascent products, the rate of passage over the barrier controlling 1,4-elimination of molecular hydrogen across the C_1–C_4 bond in **IM4** is $\sim 10^{11}$ s^{-1}, approximately an order of magnitude slower than the 1,2-elimination of H_2 from **IM1** to form cyclic products. This information provides a strong argument that the most likely isomer of $C_4H_3^+$ formed in the present experiments is the cyclic product. The results of these rate constant calculations are reported in the Supporting Information.

DISCUSSION

This study of a prototype ion–radical reaction has revealed that charge transfer is a dominant reactive pathway in such systems. However, a significant fraction, nearly 40%, of those products are formed with sufficient internal energy to result in dissociation by C–H bond cleavage. As is often observed in charge transfer processes, the electron transfer occurs on a very short time scale and at long range, resulting in energy resonance, in which the relative kinetic energies of reactant and products are unchanged.

The present study also shows that new chemical bonds, specifically new carbon–carbon bonds, may be formed, and 20% of the reaction products are formed this way. Qualitatively, the fact that the SOMO of allyl has the same b_1 symmetry as the p-orbital of C^+, suggests that the formation of a four-membered ring intermediate occurs with reasonable cross section. *Ab initio* calculations confirm this picture and suggest that elimination of molecular hydrogen from this cyclic

DOI: 10.1021/acs.jpca.6b05699
J. Phys. Chem. A 2016, 120, 6122–6128

intermediate is a plausible route for formation of the $C_4H_3^+$ products. This conclusion is bolstered by statistical rate constant calculations showing that the cyclic product is formed at least an order of magnitude more rapidly than the open-chain product.

It has been established that 1,2-elimination of H_2 from chemically activated ions often results in significant kinetic energy,[36] consistent with results reported here. In reactions 3a and 3a, the energy available to products is over 10 eV, and although the most probable kinetic energy release is observed to be ∼1 eV, product recoil distribution is quite broad and is compatible with a significant fraction of products carrying away energy in translation. We have noted that the formation of open-chain isomers of $C_4H_3^+$, shown in Figure 5b, occurs over an even larger barrier. The 1,4-elimination process requires nearly 4 eV of energy and results in an exit channel barrier of almost 2 eV. Although we have commented that the tight transition state associated with this barrier limits the rate of the open-chain isomer, a small contribution from this product may contribute to the width of the kinetic energy distribution.

Despite the large width of the kinetic energy distribution, the most probable four-carbon products are highly internally excited and undergo dissociation by C−H bond cleavage. The dramatic change in geometry as the nonplanar cyclic $C_4H_5^+$ product eliminates H_2 and forms planar $C_4H_3^+$ results in a large amount of internal excitation in the ring, which, via rapid intramolecular vibrational redistribution, results in significant C−H bond cleavage. In the present case, the majority (∼80%) of the nascent four-carbon products undergo dissociation. Not only does the large energy available to the products contribute to this high level of dissociation, but also the likely partitioning of this energy in internal excitation of the nascent products, revealed by the *ab initio* calculations as a plausible mechanism for such high vibrational excitation, is critical to understanding the decay dynamics.

CONCLUSIONS

The present study demonstrates that the reactions of ions with free radicals add to the richness of ion−neutral chemistry. In conjunction with charge transfer reactions that are of special importance in this class of reactions because of the low ionization potentials of free radicals, bond formation reactions of the type reported here may play an important role in ionic systems. These low signal level experiments have been made possible by the VMI detection method, and their interpretation has been facilitated by quantum chemical calculations of the structures of key reactive intermediates. Additional experimental studies, supported with *ab initio* calculations of the structures of important intermediates and the transition states that connect them, now appear to be feasible, and we look forward to learning new lessons in chemical reactivity as a consequence.

ASSOCIATED CONTENT

Supporting Information

The Supporting Information is available free of charge on the ACS Publications website at DOI: 10.1021/acs.jpca.6b05699.

Computed structures and energies of reaction products, intermediates, and transition states; energy dependent rate constants for isomerizations of reactive intermediates through appropriate transition states (PDF)

AUTHOR INFORMATION

Corresponding Author

*J. M. Farrar. E-mail: jfarrar@UR.rochester.edu. Telephone: (585)-275-5834.

Notes

The authors declare no competing financial interest.

ACKNOWLEDGMENTS

The authors acknowledge support for this work under National Science Foundation grants CHE-1012303 and CHE-1265406. We thank Professors Domenico Stranges, Stefano Stranges, and Stefano Falcinelli for their assistance with the design of the pyrolysis source and its implementation to produce allyl radicals and to Professor Piero Casavecchia for providing SiC pyrolysis tubes.

REFERENCES

(1) Eppink, A.; Parker, D. H. Velocity Map Imaging of Ions and Electrons Using Electrostatic Lenses: Application in Photoelectron and Photofragment Ion Imaging of Molecular Oxygen. *Rev. Sci. Instrum.* **1997**, *68*, 3477−3484.

(2) Kohn, D. W.; Clauberg, H.; Chen, P. Flash Pyrolysis Nozzle for Generation of Radicals in a Supersonic Jet Expansion. *Rev. Sci. Instrum.* **1992**, *63*, 4003−4005.

(3) Blush, J. A.; Clauberg, H.; Kohn, D. W.; Minsek, D. W.; Xu, Z.; Chen, P. Photoionization Mass and Photoelectron-Spectroscopy of Radicals, Carbenes and Biradicals. *Acc. Chem. Res.* **1992**, *25*, 385−392.

(4) Guo, Y.; Mebel, A. M.; Zhang, F.; Gu, X.; Kaiser, R. I. Crossed Molecular Beam Studies of the Reactions of Allyl Radicals, C_3H_5(X $^2A_2$), With Methylacetylene (CH_3CCH(X $^1A_1$), Allene (H_2CCCH_2(X $^1A_1$), and Their Isotopomers. *J. Phys. Chem. A* **2007**, *111*, 4914−4921.

(5) Leonori, F.; Balucani, N.; Capozza, G.; Segoloni, E.; Stranges, D.; Casavecchia, P. Crossed Beam Studies of Radical-Radical Reactions: O(^{3}P) + C_3H_5 (allyl). *Phys. Chem. Chem. Phys.* **2007**, *9*, 1307−1311.

(6) Balucani, N. Elementary Reactions and Their Role in Gas-Phase Prebiotic Chemistry. *Int. J. Mol. Sci.* **2009**, *10*, 2304−2335.

(7) Balucani, N.; Leonori, F.; Bergeat, A.; Petrucci, R.; Casavecchia, P. Crossed-Beam Dynamics Studies of the Radical-Radical Combustion Reaction O(^{3}P) + CH_3 (methyl). *Phys. Chem. Chem. Phys.* **2011**, *13*, 8322−8330.

(8) Balucani, N.; Leonori, F.; Casavecchia, P. Crossed Molecular Beam Studies of Bimolecular Reactions of Relevance in Combustion. *Energy* **2012**, *43*, 47−54.

(9) Kaiser, R. I.; Parker, D. S. N.; Mebel, A. M.; Johnson, M. A.; Martinez, T. J. Reaction Dynamics in Astrochemistry: Low-Temperature Pathways to Polycyclic Aromatic Hydrocarbons in the Interstellar Medium. *Annu. Rev. Phys. Chem.* **2015**, *66*, 43−67.

(10) Le, T. N.; Lee, H. Y.; Mebel, A. M.; Kaiser, R. I.; Ab Initio, M. O. Study of the Triplet C_3H_4 Potential Energy Surface and the Reaction of C(^{3}P) With Ethylene, C_2H_4. *J. Phys. Chem. A* **2001**, *105*, 1847−1856.

(11) Mebel, A. M.; Kaiser, R. I. Formation of Resonantly Stabilised Free Radicals via the Reactions of Atomic Carbon, Dicarbon, and Tricarbon With Unsaturated Hydrocarbons: Theory and Crossed Molecular Beams Experiments. *Int. Rev. Phys. Chem.* **2015**, *34*, 461−514.

(12) Russell, A. L.; Rohrs, H. W.; Read, D.; Giblin, D. E.; Gaspar, P. P.; Gross, M. L. Radical Cation/Radical Reactions: A Fourier Transform Ion Cyclotron Resonance Study of Allyl Radical Reacting with Aromatic Radical Cations. *Int. J. Mass Spectrom.* **2009**, *287*, 8−15.

(13) Zhang, X.; Kato, S.; Bierbaum, V. M.; Nimlos, M. R.; Ellison, G. B. Use of a Flowing Afterglow SIFT Apparatus to Study the Reactions of Ions with Organic Radicals. *J. Phys. Chem. A* **2004**, *108*, 9733−9741.

(14) Zhang, X.; Bierbaum, V. M.; Ellison, G. B.; Kato, S. Gas-Phase Reactions of Organic Radicals and Diradicals with Ions. *J. Chem. Phys.* **2004**, *120*, 3531−3534.

DOI: 10.1021/acs.jpca.6b05699
J. Phys. Chem. A 2016, 120, 6122−6128

(15) Sawyer, J. C.; Shuman, N. S.; Wiens, J. P.; Viggiano, A. A. Kinetics and Product Branching Fractions of Reactions Between a Cation and a Radical: $Ar^+ + CH_3$ and $O_2^+ + CH_3$. *J. Phys. Chem. A* **2015**, *119*, 952−958.
(16) Pei, L. S.; Carrascosa, E.; Yang, N.; Falcinelli, S.; Farrar, J. M. Velocity Map Imaging Study of Charge-Transfer and Proton-Transfer Reactions of CH_3 Radicals with H_3^+. *J. Phys. Chem. Lett.* **2015**, *6*, 1684−1689.
(17) Carpenter, M. A.; Zanni, M. T.; Levandier, D. J.; Varley, D. F.; Farrar, J. M. Proton Transfer Dynamics on Highly Attractive Potential Energy Surfaces: Induced Repulsive Energy Release in O^- + HF at High Collision Energies. *Can. J. Chem.* **1994**, *72*, 828−835.
(18) Thermodynamic parameters taken from NIST Chemistry Webbook; Mallard, W. G., Linstrom, P. J., Eds.; NIST Standard Database Number 69; National Institute of Standards and Technology: Gaithersburg, MD, 2000 (http://webbook.nist.gov/chemistry/).
(19) Pei, L.; Farrar, J. M. Imaging Ion−Molecule Reactions: Charge Transfer and C-N Bond Formation in the $C^+ + NH_3$ System. *J. Chem. Phys.* **2012**, *136*, 204305.
(20) Pei, L.; Farrar, J. M. Ion Imaging Study of Reaction Dynamics in the $N^+ + CH_4$ System. *J. Chem. Phys.* **2012**, *137*, 154312.
(21) Stei, M.; von Vangerow, J.; Otto, R.; Kelkar, A. H.; Carrascosa, E.; Best, T.; Wester, R. High Resolution Spatial Map Imaging of a Gaseous Target. *J. Chem. Phys.* **2013**, *138*, 214201.
(22) Guan, Q.; Urness, K. N.; Ormond, T. K.; David, D. E.; Ellison, G. B.; Daily, J. W. The Properties of a Micro-Reactor for the Study of the Unimolecular Decomposition of Large Molecules. *Int. Rev. Phys. Chem.* **2014**, *33*, 447−487.
(23) Cunha de Miranda, B. K.; Alcaraz, C.; Elhanine, M.; Noller, B.; Hemberger, P.; Fischer, I.; Garcia, G. A.; Soldi-Lose, H.; Gans, B.; Vieira Mendes, L. A.; et al. Threshold Photoelectron Spectroscopy of the Methyl Radical Isotopomers, CH_3, CH_2D, CHD_2 and CD_3: Synergy between VUV Synchrotron Radiation Experiments and Explicitly Correlated Coupled Cluster Calculations. *J. Phys. Chem. A* **2010**, *114*, 4818−4830.
(24) Udseth, H.; Giese, C. F.; Gentry, W. R. Transition Probabilities and Differential Cross-Sections for Vibrational Excitation in Collisions of H^+ with H_2, HD, and D_2. *Phys. Rev. A: At., Mol., Opt. Phys.* **1973**, *8*, 2483−2493.
(25) Lao, R. C. C.; Rozett, R. W.; Koski, W. S. Ion−Molecule Reactions of C^+ with N_2 and O_2. *J. Chem. Phys.* **1968**, *49*, 4202−4209.
(26) Smith, R. D.; Futrell, J. H. Ion−Molecule Reaction-Mechanisms - Thermal-Energy Gas-Phase Reactions of $C\text{-}12^+$ and $C\text{-}13^+$ Ions With CH_4, C_2H_4, C_2H_6, C_3H_6, C_3H_8, and $CD_3CH_2CD_3$. *J. Chem. Phys.* **1976**, *65*, 2574−2583.
(27) Friedrich, B.; Herman, Z. Processing of Ion−Molecule Beam Scattering Data: Framework of Scattering Diagrams and Derived Quantities. *Collect. Czech. Chem. Commun.* **1984**, *49*, 570−585.
(28) Dribinski, V.; Ossadtchi, A.; Mandelshtam, V. A.; Reisler, H. Reconstruction of Abel-Transformable Images: The Gaussian Basis-Set Expansion Abel Transform Method. *Rev. Sci. Instrum.* **2002**, *73*, 2634−2642.
(29) Herman, Z.; Futrell, J. H.; Friedrich, B. A Beam Scattering Study of the Collision-Induced Dissociation of Polyatomic Ions CH_4^+ and $C_3H_8^+$ at eV Collision Energies. *Int. J. Mass Spectrom. Ion Processes* **1984**, *58*, 181−199.
(30) Shukla, A. K.; Qian, K. G.; Howard, S. L.; Anderson, S. G.; Sohlberg, K. W.; Futrell, J. H. Collision-Induced Dissociation Reaction Dynamics of the Acetone Molecular Ion. *Int. J. Mass Spectrom. Ion Processes* **1989**, *92*, 147−169.
(31) Shukla, A. K.; Qian, K.; Anderson, S.; Futrell, J. H. Fundamentals of Tandem Mass-Spectrometry - a Dynamics Study of Simple C-C Bond-Cleavage in Collision-Activated Dissociation of Polyatomic Ions At Low-Energy. *J. Am. Soc. Mass Spectrom.* **1990**, *1*, 6−15.
(32) Cunje, A.; Rodriquez, C. F.; Lien, M. H.; C, H. A. The $C_4H_5^+$ Potential Energy Surface: Structure, Relative Energies, and Enthalpies of Formation of Isomers of $C_4H_5^+$. *J. Org. Chem.* **1996**, *61*, 5212−5220.
(33) Frisch, M. J.; Trucks, G. W.; Schlegel, H. B.; Scuseria, G. E.; Robb, M. A.; Cheeseman, J. R.; J. A. Montgomery, J.; Vreven, T.; Kudin, K. N.; Burant, J. C., et al. *Gaussian 03*, C.02; Gaussian, Inc.: Wallingford, CT, 2004.
(34) Lang, M.; Holzmeier, F.; Hemberger, P.; Fischer, I. Threshold Photoelectron Spectra of Combustion Relevant C_4H_5 and C_4H_7 Isomers. *J. Phys. Chem. A* **2015**, *119*, 3995−4000.
(35) Marcus, R. A. Unimolecular Dissociations and Free Radical Recombination Reactions. *J. Chem. Phys.* **1952**, *20*, 359−364.
(36) Uggerud, E. Translational energy release: Experiment and theory. H_2 elimination reactions of small gas phase ions, and correspondence to H-H bond activation. *Mass Spectrom. Rev.* **1999**, *18*, 285−308.

DOI: 10.1021/acs.jpca.6b05699
J. Phys. Chem. A 2016, 120, 6122−6128